Highly polar bonds and the meaning of covalency and ionicity—structure and bonding of alkali metal hydride oligomers

F. Matthias Bickelhaupt,*[a] Miquel Solà*[b] and Célia Fonseca Guerra[a]

Received 28th April 2006, Accepted 14th June 2006
First published as an Advance Article on the web 14th September 2006
DOI: 10.1039/b606093e

The hydrogen–alkali metal bond is simple and archetypal, and thus an ideal model for studying the nature of highly polar element–metal bonds. Thus, we have theoretically explored the alkali metal hydride monomers, HM, and (distorted) cubic tetramers, $(HM)_4$, with M = Li, Na, K, and Rb, using density functional theory (DFT) at the BP86/TZ2P level. Our objective is to determine how the structure and thermochemistry (*e.g.*, H–M bond lengths and strengths, oligomerization energies, *etc.*) of alkali metal hydrides depend on the metal atom, and to understand the emerging trends in terms of quantitative Kohn–Sham molecular orbital (KS-MO) theory. The H–M bond becomes longer and weaker, both in the monomers and tetramers, if one descends the periodic table from Li to Rb. Quantitative bonding analyses show that this trend is not determined by decreasing electrostatic attraction but, primarily, by the weakening in orbital interactions. The latter become less stabilizing along Li–Rb because the bond overlap between the singly occupied molecular orbitals (SOMOs) of $H^\bullet$ and $M^\bullet$ radicals decreases as the metal *n*s atomic orbital (AO) becomes larger and more diffuse. Thus, the H–M bond behaves as a text-book electron-pair bond and, in that respect, it is covalent, despite a high polarity. For the lithium and sodium hydride tetramers, the H_4 tetrahedron is larger than and surrounds the M_4 cluster (*i.e.*, H–H > M–M). Interestingly, this is no longer the case in the potassium and rubidium hydride tetramers, in which the H_4 tetrahedron is *smaller* than and inside the M_4 cluster (*i.e.*, H–H < M–M).

1. Introduction

Alkali metal hydrides, H_mM_n with M = Li to Rb, have received considerable attention in recent years,[1–6] amongst others, because their investigation provides insight into how nonlinear optical properties vary with cluster size and also because of potential technological applications in the field of hydrogen storage.[2,3] Alkali metal and in particular lithium hydride oligomers are models for simple electron-deficient metal compounds featuring multicenter bonding.[4] Lithium hydride is also

[a] *Afdeling Theoretische Chemie, Scheikundig Laboratorium der Vrije Universiteit, De Boelelaan 1083, NL-1081 HV Amsterdam, The Netherlands. E-mail: FM.Bickelhaupt@few.vu.nl; Fax: +31 20 59 87 629*
[b] *Institut de Química Computacional, Universitat de Girona, Campus Montilivi, E-17071 Girona, Catalonia, Spain. E-mail: miquel.sola@udg.es; Fax: +34 972 41 83 56*

the smallest heteronuclear diatomic molecule and thus an ideal model for studying the nature of polar bonds,[5] the main purpose of this work. Structural and thermochemical data about alkali metal hydride oligomers $(HM)_n$ are still incomplete in spite of various pioneering experimental (only for monomers HM)[7] and theoretical[4,5,8] investigations. The tetramer $(HM)_4$ is, apart from the monomers, the most widely studied oligomer, in particular for M = Li. It is the smallest stable cluster that may form a compact cubic lattice fragment (**1**) but also other isomers such as the ladder (**2**) and ring (**3**) are possible.

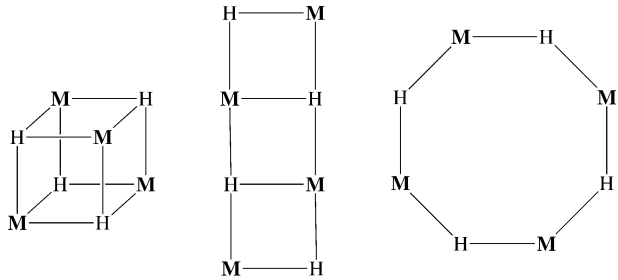

1 **2** **3**

Most theoretical studies (except for early work by Kato and coworkers)[4,8i,j] agree that the lowest-energy isomer of $(HLi)_4$ and $(HNa)_4$ is the cube (**1**), especially when correlation effects are included in the calculations.[5a,8b,d]

The purpose of the present study is twofold. First, we aim at a better understanding of the nature of highly polar chemical bonds. This is inspired by our recent finding that the C–M bond in methylalkali metal oligomers has substantial covalent character which is essential for understanding trends in bond strengths.[9] Here, we wish to clarify if such covalent character is also present in the H–M bond in alkali metal hydrides, which are of a similar polarity as the C–M bond. An asset of the hydrogen–alkali metal bond is that it is simple and archetypal, and thus an ideal model for obtaining insight into the nature of highly polar element–metal bonds in general. Thus, we have undertaken a detailed investigation of alkali metal hydride monomers HM and tetramers $(HM)_4$ with M = Li, Na, K and Rb, using the generalized gradient approximation (GGA) of Density Functional Theory (DFT) at the BP86/TZ2P level of theory.[10,11] The polar H–M bonds are analyzed in the framework of the Kohn–Sham molecular orbital (KS-MO) model using a quantitative bond energy decomposition.[10]

A striking result of our analyses is that the reduction of the bond overlap between the singly-occupied hydrogen 1s and metal *n*s atomic orbitals and the concomitant loss in orbital interactions is the dominant factor determining the reduction in H–M bond strength if one goes from HLi to the heavier metal hydrides, and not the loss in electrostatic interactions. Nevertheless, the H–M bonds are highly polar. This also leads to the more general insight that one must distinguish between covalent or ionic features in the *bonding mechanism* on one hand and the *polarity of the charge distribution* on the other.

A second objective is to obtain a set of consistent structural and thermochemical data for alkali metal hydride monomers HM and tetramers (geometries, H–M bond strengths, tetramerization energies), all obtained with exactly the same GGA density functional method. This complements the available experimental and theoretical data, which are scarce or even missing for the tetramers of the heavier alkali metal systems (beyond sodium), and enables a systematic analysis of the trends. In this context, we note that experimental information on isolated tetramers is not available, and only very recently an Li_4H_4 cube coordinated to three bis(amino)alane units has been synthesized.[7g] For the tetramers, we focus on this cubic isomer, which is in general not a perfect but a distorted cube. In $(HLi)_4$, for example, the lithium atoms constitute an inner cluster that is surrounded by four hydrogen atoms, one on

each face of the tetrahedral metal cluster (**4**), similar to the situation for tetramethyllithium (**5**).[9b]

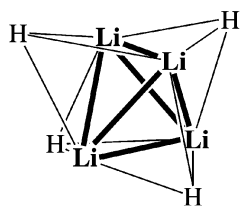

4

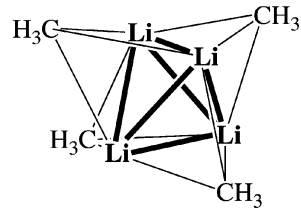

5

An interesting structural phenomenon that we find is the change of relative size of the hydride tetrahedron and the metal cluster if one goes from sodium to potassium. Thus, for the heavier alkali metals K and Rb, the H_4 unit is inside the M_4 cluster.

2. Theoretical methods

2.1. General procedure

All calculations were performed using the Amsterdam Density Functional (ADF) program.[11] The numerical integration was carried out using the procedure developed by Boerrigter, te Velde, and Baerends.[11e,f] The molecular orbitals (MO) were expanded in a large uncontracted set of Slater type orbitals (STOs) containing diffuse functions, which is of triple-ζ quality for all atoms and has been augmented with two sets of polarization functions: 2p and 3d on H; 3d and 4f on Li, and Na; 4d and 4f on K and Rb.[11g] In addition, an extra set of p functions was added to the basis sets of Li (2p), Na (3p), K (4p) and Rb (5p). The 1s core shell of lithium, the 1s 2s 2p core shells of sodium and potassium, and the 1s 2s 3s 2p 3p 3d core shells of rubidium were treated by the frozen-core approximation.[11d] An auxiliary set of s, p, d, f, and g STOs was used to fit the molecular density and to represent the Coulomb and exchange–correlation potentials accurately in each SCF cycle.[11h]

Energies, geometries[12] and frequencies[13] were computed using the generalized gradient approximation (GGA) of DFT at the BP86 level.[14] All open-shell systems were treated with the spin-unrestricted formalism.

Bond enthalpies at 298.15 K and 1 atmosphere (ΔH_{298}) were calculated from electronic bond energies (ΔE) according to eqn (1), assuming an ideal gas.[15]

$$\Delta H_{298} = \Delta E + \Delta E_{\mathrm{trans},298} + \Delta E_{\mathrm{rot},298} + \Delta E_{\mathrm{vib},0} + \Delta(\Delta E_{\mathrm{vib},0})_{298} + \Delta(pV) \qquad (1)$$

Here, $\Delta E_{\mathrm{trans},298}$, $\Delta E_{\mathrm{rot},298}$ and $\Delta E_{\mathrm{vib},0}$ are the differences between products and reactants in translational, rotational and zero point vibrational energy, respectively; $\Delta(\Delta E_{\mathrm{vib}})_{298}$ is the change in the vibrational energy difference as one goes from 0 to 298.15 K. The vibrational energy corrections are based on our frequency calculations. The molar work term $\Delta(pV)$ is $(\Delta n)RT$ (*e.g.*, for two fragments combining to one molecule $\Delta n = -1$). Thermal corrections for the electronic energy are neglected.

2.2. Bond energy decomposition

The overall bond energy ΔE is made up of two major components (eqn (2)):

$$\Delta E = \Delta E_{\mathrm{prep}} + \Delta E_{\mathrm{int}} \qquad (2)$$

In this formula, the preparation energy ΔE_{prep} is the amount of energy required to deform the separate molecular fragments that are connected by the chemical bond from their equilibrium structure to the geometry that they acquire in the overall molecular system. The interaction energy ΔE_{int} corresponds to the actual energy change when the prepared fragments are combined to form the overall molecule. It is analyzed for our model systems in the framework of the Kohn–Sham MO model

using a Morokuma-type decomposition of the bond into electrostatic interaction, exchange repulsion (or Pauli repulsion), and (attractive) orbital interactions (eqn (3)).[10,16]

$$\Delta E_{\mathrm{int}} = \Delta V_{\mathrm{elstat}} + \Delta E_{\mathrm{Pauli}} + \Delta E_{\mathrm{oi}} \tag{3}$$

The term $\Delta V_{\mathrm{elstat}}$ corresponds to the classical electrostatic interaction between the unperturbed charge distributions of the prepared (*i.e.* deformed) bases and is usually attractive. The Pauli repulsion $\Delta E_{\mathrm{Pauli}}$ comprises the destabilizing interactions between occupied orbitals. It arises as the energy change associated with going from the superposition of the unperturbed electron densities of two fragments, say $H^{\bullet}$ and $M^{\bullet}$, *i.e.*, $\rho_{H(\alpha)} + \rho_{M(\beta)}$, to the wavefunction $\Psi^0 = N\hat{A}\,[\Psi_{H(\alpha)}\,\Psi_{M(\beta)}]$, that properly obeys the Pauli principle through explicit antisymmetrization ($\hat{A}$ operator) and renormalization (N constant) of the product of fragment wavefunctions.[10] It comprises the four-electron destabilizing interactions between occupied orbitals and is responsible for any steric repulsion. The orbital interaction ΔE_{oi} in any MO model, and therefore also in Kohn–Sham theory, accounts for electron-pair bonding, charge transfer (*i.e.*, donor–acceptor interactions between occupied orbitals on one fragment with unoccupied orbitals of the other, including the HOMO–LUMO interactions) and polarization (empty–occupied orbital mixing on one fragment due to the presence of another fragment). In the case of open-shell fragments, the bond energy analysis yields, for technical reasons, interaction energies that differ consistently in the order of a kcal mol^{-1} (too much stabilizing) from the exact BP86 result (because, only in the bond energy analysis, the spin-polarization in the fragments is not accounted for). To facilitate a straightforward comparison, the results of the bond energy analysis were scaled to match exactly the regular BP86 bond energies.

The orbital interaction energy can be decomposed into the contributions from each irreducible representation Γ of the interacting system (eqn (4)) using the extended transition state (ETS) scheme developed by Ziegler and Rauk.[16d,e]

$$\Delta E_{\mathrm{oi}} = \Sigma_{\Gamma} \Delta E_{\Gamma} \tag{4}$$

2.3. Analysis of the charge distribution

The electron density distribution is analyzed using the Voronoi deformation density (VDD) method[17,18] and the Hirshfeld scheme[19] for computing atomic charges. The VDD atomic charge $Q_{\mathrm{A}}^{\mathrm{VDD}}$ is computed as the (numerical) integral[11f] of the deformation density $\Delta\rho(\boldsymbol{r}) = \rho(\boldsymbol{r}) - \Sigma_{\mathrm{B}}\,\rho_{\mathrm{B}}(\boldsymbol{r})$ in the volume of the Voronoi cell of atom A (eqn (5)). The Voronoi cell of atom A is defined as the compartment of space bounded by the bond midplanes on and perpendicular to all bond axes between nucleus A and its neighboring nuclei (*cf.* the Wigner–Seitz cells in crystals[18c]).

$$Q_{\mathrm{A}}^{\mathrm{VDD}} = -\int_{\text{Voronoi cell of A}} \left(\rho(\boldsymbol{r}) - \sum_{\mathrm{B}} \rho_{\mathrm{B}}(\boldsymbol{r})\right) \mathrm{d}\boldsymbol{r} \tag{5}$$

Here, $\rho(\boldsymbol{r})$ is the electron density of the molecule and $\Sigma_{\mathrm{B}}\rho_{\mathrm{B}}(\boldsymbol{r})$ the superposition of atomic densities $\rho_{\mathrm{B}}(\boldsymbol{r})$ of a fictitious promolecule without chemical interactions that is associated with the situation in which all atoms are neutral. The interpretation of the VDD charge $Q_{\mathrm{A}}^{\mathrm{VDD}}$ is rather straightforward and transparent. Instead of measuring the amount of charge associated with a particular atom A, $Q_{\mathrm{A}}^{\mathrm{VDD}}$ directly monitors how much charge flows, due to chemical interactions, out of ($Q_{\mathrm{A}}^{\mathrm{VDD}} > 0$) or into ($Q_{\mathrm{A}}^{\mathrm{VDD}} < 0$) the Voronoi cell of atom A, that is, the region of space that is closer to nucleus A than to any other nucleus.

3. Results and discussion

3.1. Structures

Monomers. The computed BP86/TZ2P geometries are summarized in Table 1 and illustrated in Fig. 1. The H–M bond distance in the diatomic alkali metal hydride monomers increases systematically from 1.629, to 1.935, to 2.310 to 2.405 Å along M = Li, Na, K and Rb, respectively. Note that the increase in bond length in every step becomes smaller as one descends the periodic table.

Our results agree satisfactorily with earlier theoretical[5,8a,c,e,f,h] and high-resolution infrared experimental studies,[7a–d] which also yield a monotonic increase of the H–M bond along HLi, HNa, HK and HRb (Table 1). CCSD(T) calculations[8a] are only available for H–Li; depending on the basis set employed, they yield H–Li bond distances of 1.592–1.608 Å, which are shorter than our BP86/TZ2P result by 1–2%.

Table 1 Structures (in Å) of alkali metal hydride monomers and tetramers[a]

System	Method	H–M	M–M	H–H	Ref.
HLi	BP86/TZ2P	1.629	—	—	This work
	ROHF/6-311G**	1.607	—	—	8*c*
	BLYP/6-311G**	1.600	—	—	8*c*
	MP2/6-31++G**	1.625	—	—	8*f*
	VB/6-311G**	1.621	—	—	5*b*
	CCSD(T)/cc-pV(5,Q)Z+aug(H,F)	1.6081	—	—	8*a*
	CCSD(T)/MT(ae)	1.5923	—	—	8*a*
	DHFR + CI[c]	1.588	—	—	8*e*
	Exp.	1.5949	—	—	7*a*,*b*
$(HLi)_4$	BP86/TZ2P	1.879	2.525	2.777	This work
	HF/5-21G	1.901	2.607	2.764	4,8*i*
	HF/ECPs	1.87	—[b]	—[b]	8*b*
	HF/H(5s1p/3s1p) + Li(7s1p/3s1p)	1.86	2.49	2.75	8*d*
	B3LYP/6-311G**	1.90	2.464	—[b]	8*g*,*h*
HNa	BP86/TZ2P	1.935	—	—	This work
	MP2/6-31++G**	1.915	—	—	8*f*
	DHFR + CI[c]	1.865	—	—	8*e*
	MCSCF/TZP	1.910	—	—	8*k*
	Exp.	1.8874	—	—	7*c*,*d*
$(HNa)_4$	BP86/TZ2P	2.300	3.155	3.345	This work
	HF/H(5s1p/3s1p) + Na(9s6p/5s3p)	2.25	3.10	3.28	8*d*
HK	BP86/TZ2P	2.310	—	—	This work
	MP2/ECP	2.261	—	—	8*f*
	DHFR + CI[c]	2.223	—	—	8*e*
	Exp.	2.240	—	—	7*c*,*d*
$(HK)_4$	BP86/TZ2P	2.656	3.783	3.729	This work
HRb	BP86/TZ2P	2.405	—	—	This work
	MP2/ECP	2.546	—	—	8*f*
	DHFR + CI[c]	2.311	—	—	8*e*
	Exp.	2.367	—	—	7*c*,*d*
$(HRb)_4$	BP86/TZ2P	2.774	3.939	3.907	This work

[a] At BP86/TZ2P. [b] Not specified in reference. [c] Dirac–Hartree–Fock–Roothaan calculations.

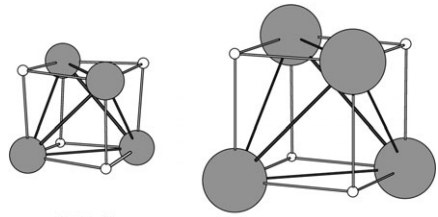

Fig. 1 Structures (on scale) of alkali metal hydride tetramers for lithium and rubidium (for numerical results, see Table 1).

The experimental values for the H–M bond distances are 2–3% shorter than our values.

Tetramers. Tetramerization causes the H–M bond to expand by 0.25 (Li)−0.37 Å (Rb) as can be seen in Table 1. Thus, the H–M bond in the T_d symmetric alkali metal hydride tetramers increases monotonically if one descends the periodic table from 1.879 (Li) to 2.300 (Na) to 2.656 (K) to 2.774 Å (Rb), similar to the monomers but at somewhat larger values than in the latter.

A striking structural phenomenon is the change of relative size of the hydride tetrahedron and the metal cluster if one goes from sodium to potassium. Thus, for Li and Na, the H_4 unit is outside the M_4 cluster (*i.e.* H–H > M–M) similar to the situation found for methyllithium and methylsodium tetramers.[9b] However, for the heavier alkali metals K and Rb, the H_4 unit is inside the M_4 cluster (*i.e.* H–H < M–M), as illustrated by Fig. 1. At variance, in the methylalkali metal tetramers, the metal cluster is always smaller than the surrounding cage of four methyl groups, also for potassium and rubidium. This can be ascribed to the larger steric demand of a CH_3 group as compared to a H atom.

We are not aware of any experimental data on the geometry parameters of alkali metal hydride tetramers. This prevents a comparison of structural trends found by us with experiment. Other theoretical investigations[4,8b,d,g,h,i] are limited to $(HLi)_4$ and $(HNa)_4$. The latter molecule is only considered in the Hartree–Fock study by Rupp and Ahlrichs,[8d] which confirms the H–M bond elongation going from $(HLi)_4$ to $(HNa)_4$.

3.2. Thermochemistry

Monomers. The thermochemical results of our BP86/TZ2P calculations are collected in Table 2 (monomers) and 3 (tetramers). Homolytic dissociation of the H–M bond in alkali metal hydride monomers (*i.e.*, $HM \rightarrow H^{\bullet} + M^{\bullet}$) is favored over heterolytic or ionic dissociation (*i.e.*, $HM \rightarrow H^{-} + M^{+}$) for all alkali metal hydride monomers with heterolytic bond dissociation enthalpies (BDE = $-\Delta H$ in Table 2) being 2.9–3.4 times higher than the homolytic ones. This is because charge separation is energetically highly unfavorable in the gas phase. The H–M bond strength decreases markedly if one goes from lithium to the heavier alkali metals and decays more slowly along the latter. For example, the homolytic BDE is −55.5, −43.4, −40.6 and −39.4 kcal mol^{-1} along M = Li, Na, K and Rb (see ΔH_{homo} in Table 2). This finding is remarkable because it is *not* in line with the idea of an "ionic" hydrogen–alkali metal bond. We will come back to this in Section 3.3.

Our homolytic bond dissociation energies ΔE_{homo} agree excellently with experimental[7c,d] values (which differ by only 1–2 kcal mol^{-1}) and other theoretical[8c,e,f,k,l] values (*e.g.*, G2 values[8l] for HLi and HNa, which differ by less than 1 kcal mol^{-1}). They all confirm the monotonic decrease in H–M bond strength along M = Li–Rb.

Table 2 Homolytic and heterolytic H–M bond strength (in kcal mol^{-1}) of alkali metal hydride monomers

		Bond energies[b]		Bond enthalpies[c]		
Species	Method[a]	ΔE_{homo}	ΔE_{hetero}	ΔH_{homo}	ΔH_{hetero}	Ref.
HLi	BP86/TZ2P	−56.5	−165.9	−55.5	−164.9	This work
	ROHF/6-311G**	−33.9	—[d]	—[d]	—[d]	8*c*
	BLYP/6-311G**	−57.9	—[d]	—[d]	—[d]	8*c*
	VB	−49.2	—[d]	—[d]	—[d]	5*b*
	DHFR + CI[e]	−57.5	—[d]	—[d]	—[d]	8*e*
	G2	−56.6	—[d]	—[d]	—[d]	8*l*
	UB3LYP//MP2/6-31 + + G**	−58.0[f]	—[d]	—[d]	—[d]	8*f*
	Exp.	−58.0	—[d]	—[d]	—[d]	7*c*,*d*
HNa	BP86/TZ2P	−44.1	−148.8	−43.4	−148.1	This work
	DHFR + CI[e]	−45.9	—[d]	—[d]	—[d]	8*e*
	MCSCF/TZP	−43.3	—[d]	—[d]	—[d]	8*k*
	G2	−45.0	—[d]	—[d]	—[d]	8*l*
	UB3LYP//MP2/6-31 + + G**	−45.3[f]	—[d]	—[d]	—[d]	8*f*
	Exp.	−45.5	—[d]	—[d]	—[d]	7*c*,*d*
HK	BP86/TZ2P	−41.1	−125.4	−40.6	−124.9	This work
	DHFR + CI[e]	−42.7	—[d]	—[d]	—[d]	8*e*
	UB3LYP//MP2/ECP	−42.6[f]	—[d]	—[d]	—[d]	8*f*
	Exp.	−42.2	—[d]	—[d]	—[d]	7*c*,*d*
HRb	BP86/TZ2P	−39.9	−119.4	−39.4	−118.9	This work
	UB3LYP//MP2/ECP	−40.1[f]	—[d]	—[d]	—[d]	8*f*
	DHFR + CI[e]	−42.3	—[d]	—[d]	—[d]	8*e*
	Exp.	−41.7	—[d]	—[d]	—[d]	7*c*,*d*

[a] Energy and structure obtained at the same level of theory. [b] Electronic energies. [c] 298.15 K enthalpies. [d] Not specified in reference. [e] Dirac–Hartree–Fock–Roothaan calculations. [f] Electronic energies + ZPE.

Tetramers. Tetramerization is considerably more exothermic for lithium hydride than for the heavier alkali metal hydride tetramers (see Table 3). The tetramerization enthalpy of HM molecules is −130.5, −93.4, −97.8 and −94.0 kcal mol^{-1} along M = Li, Na, K and Rb. These ΔH_{tetra} values are also more stabilizing than those of

Table 3 Tetramerization energies and enthalpies (in kcal mol^{-1}) of alkali metal hydride monomers

Monomer	Method[a]	ΔE_{tetra}[b]	ΔH_{tetra}[c]	Ref.
HLi	BP86/TZ2P	−136.5	−130.5	This work
	HF/H(5s1p/3s1p) + Li(7s1p/3s1p)	−139.0	—[d]	8*d*
	MP2//RHF/SVP	−146.6	—[d]	8*n*
	CEPA/H(5s/3s) + Li(7s/3s)	−143.9	—[d]	8*d*
HNa	BP86/TZ2P	−97.0	−93.4	This work
	HF/H(5s1p/3s1p) + Na(9s6p/5s3p)	−117.5	—[d]	8*d*
HK	BP86/TZ2P	−101.3	−97.8	This work
HRb	BP86/TZ2P	−97.3	−94.0	This work

[a] Energy and structure obtained at the same level of theory. [b] Electronic energies. [c] 298.15 K enthalpies. [d] Not specified in reference.

the corresponding methylalkali metal molecules CH_3M which amount to −120.3, −73.5, −82.5, −87.1 kcal mol^{-1}, respectively.[9b]

There are no experimental tetramerization energies for alkali metal hydrides to which we could compare our own results. Other theoretical values have been computed only for HLi and HNa, for the latter molecule only at the Hartree–Fock level.[8d] The Hartree–Fock values are 3–21 kcal mol^{-1} more binding than our BP86 values but they confirm the decrease of the tetramerization energy going from HLi to HNa. The CEPA and MP2 values for the tetramerization energy of HLi are more stabilizing than our BP86 value by 7–10 kcal mol^{-1}.[8d,n]

3.3. Analysis of the H–M bond in alkali metal hydride monomers

Electronic structure and bonding mechanism. The analyses of the electronic structure and bonding mechanisms in alkali metal hydride monomers HM reveal substantial covalent character for the H–M bond (see Table 4 and Fig. 2) and, at the same time, a high polarity (see also the section on "Heterolytic Bond Dissociation", below). In the first place, for all four alkali metals, the H–M bond is characterized by substantial mixing between the hydrogen 1s AO and the alkali metal *n*s AO in the 1s + *n*s electron-pair bonding combination (see Fig. 2). While it is true that the electron-pair bonding 1*n* + *n*s combination is polarized toward hydrogen, the alkali metal *n*s contribution is significant and not at all marginal: in terms of Gross Mulliken contributions[21] the composition is approximately 60% 1s + 25% *n*s (see

Table 4 Analysis of the H–M bond between H$^\bullet$ and M$^\bullet$ in alkali metal hydride monomers[a]

	H–Li	H–Na	H–K	H–Rb
Bond energy decomposition/kcal mol^{-1}				
ΔE_σ	−52.7	−40.4	−39.2	−39.5
ΔE_π	0.0	0.0	0.0	0.0
ΔE_{oi}	−52.7 (−43.5)[b]	−40.4 (−37.9)[b]	−39.2 (−32.0)[b]	−39.5 (−34.1)[b]
ΔE_{Pauli}	3.2	5.0	5.6	7.7
ΔV_{elstat}	−7.0	−8.7	−7.5	−8.1
$\Delta E_{int} = \Delta E_{homo}$	−56.5 (−47.3)[b]	−44.1 (−41.6)[b]	−41.1 (−33.9)[b]	−39.9 (−34.5)[b]
Fragment orbital overlaps $\langle H \mid M \rangle$				
$\langle 1s \mid ns \rangle$[c]	0.51	0.44	0.37	0.35
$\langle 1s \mid np_\sigma \rangle$[c]	0.56	0.54	0.47	0.46
Fragment orbital interaction matrix elements $\langle H \mid F \mid M \rangle$/kcal mol^{-1}				
$\langle 1s \mid F \mid ns \rangle$[c,d]	−66.5	−60.9	−43.7	—[d]
Fragment orbital populations (in electrons)				
H				
1s	1.18	1.27	1.36	1.25
M				
ns[c]	0.53	0.58	0.45	0.50
np_σ[c]	0.29	0.10	0.09	0.15

[a] At BP86/TZ2P. See Section 2.3 for explanation of energy terms. [b] All virtual fragment orbitals deleted. [c] n = 2, 3, 4 and 5 for M = Li, Na, K and Rb. [d] Computed with the fully converged SCF density of HM. Cannot yet be computed for Rb, for technical reasons.

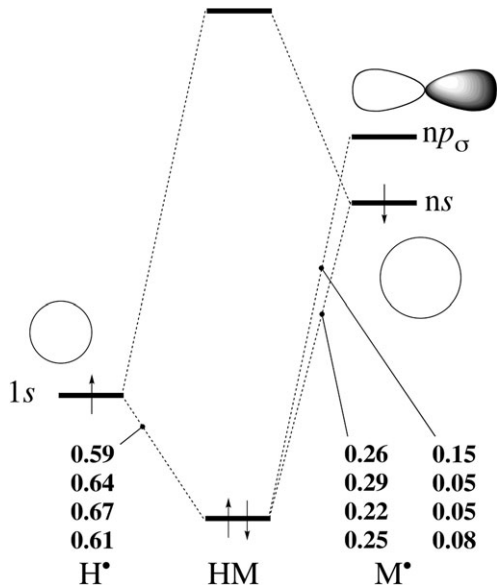

Fig. 2 Orbital interaction diagram for HM with Gross Mulliken contributions at BP86/TZ2P of H• and M• fragment orbitals to the H–M electron-pair bonding MO for M = Li, Na, K and Rb.

Fig. 2). In the case of lithium hydride, the situation is 59% 1s + 26% 2s with, in addition, a sizeable contribution of 15% from the lithium $2p_\sigma$ AO. In terms of mixing coefficients, this is 0.61 1s + 0.40 2s ($+0.25$ $2p_\sigma$).

The above mixing is indicative for substantial 1s + *n*s orbital interaction, which is confirmed by further analyses. Indeed, the bond interaction–matrix elements $F_{\text{bond}} = \langle 1s|F|ns\rangle$ between the two SOMOs are strongly stabilizing with values ranging from -66.5 (Li) to -60.9 (Na) to -43.7 kcal mol^{-1} (K) (see Table 4; *F* is the effective one-electron Hamiltonian or Fock operator evaluated with the fully converged SCF density of the molecule). We recall that the stabilization $\Delta\varepsilon$ of our electron-pair bonding 1s + *n*s combination with respect to ε(1s) is, in second order (and neglecting the effect of other occupied and virtual orbitals!), given by $\langle 1s\,|F|\,ns\rangle^2/\varepsilon(1s) - \varepsilon(ns)$, that is, the interaction–matrix element squared divided by the difference in orbital energies.[22] Thus, according to this approximate relationship, the stabilization $\Delta\varepsilon$ is a sizeable 45 kcal mol^{-1} for the H–Li bond, 36 kcal mol^{-1} for the H–Na bond and 17 kcal mol^{-1} for the H–K bond (see ε(1s), ε(*n*s) and $\langle 1s|F|ns\rangle$ values in Fig. 3 and Table 4). This is a weakening along the H–Li, H–Na and H–K bonds.

This trend can be straightforwardly understood in terms of the corresponding bond overlap $S_{\text{bond}} = \langle 1s \mid ns\rangle$, which is sizeable and decreases from 0.51 to 0.44 to 0.37 to 0.35 along M = Li, Na, K and Rb (see Table 4). This is caused by the metal

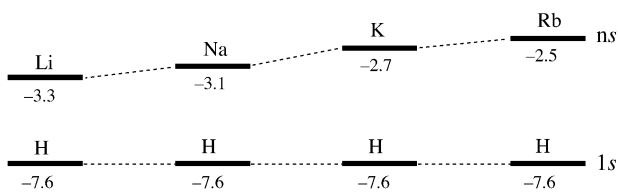

Fig. 3 Energies (in eV) of the SOMOs of hydrogen H• and alkali metal M• atoms at BP86/TZ2P.

*n*s AOs becoming more diffuse and extended along this series, leading to smaller optimum overlap at longer bond distance.[23] This mechanism, which causes the C–M bond to weaken along Li, Na, K as observed, is illustrated by **6** and **7**, below:

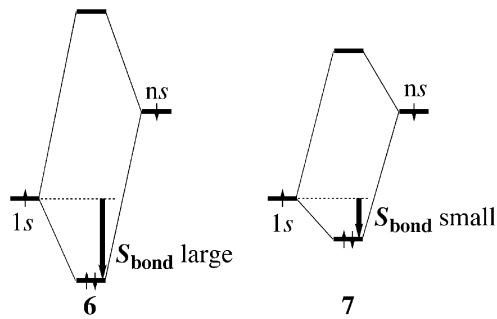

6 **7**

These illustrations show how the stabilization of the electrons in the bonding 1s + *n*s combination is reduced if one goes from a situation with stronger (**6**) to a situation with weaker (**7**) $\langle 1s \mid ns \rangle$ overlap and orbital interaction.

The above picture is confirmed by our quantitative bond energy decomposition. The exact (within our Kohn–Sham MO approach) values of the orbital interactions ΔE_{oi} differ of course from the above estimates. But, importantly, they are also of decisive importance *and* they show again the same trend. Along the H–Li, H–Na and H–K bonds, the orbital interactions ΔE_{oi} weaken from −52.7 to −40.4 to −39.2 kcal mol^{-1}. The same holds true for the pure orbital–interaction effect of forming the electron-pair bonding combination between the 1s and *n*s SOMOs. This effect has been isolated from the full orbital interactions ΔE_{oi} by carrying out the bond energy analysis in the absence of any virtual hydrogen and alkali metal fragment orbitals. The resulting electron-pair bonding energies ΔE_{ep} (shown in parentheses next to ΔE_{oi} values in Table 4) weaken along Li, Na and K, namely from −43.5 to −37.9 to −32.0 kcal mol^{-1}, thus nicely correlating with the decreasing $\langle 1s \mid ns \rangle$ bond overlap. The deletion of virtual fragment orbitals has no effect on ΔV_{elstat} and ΔE_{Pauli} because they only depend on the occupied fragment orbitals. Note that the trend resulting from the orbital interactions ΔE_{oi} is affected *neither* by the electrostatic attraction ΔV_{elstat} *nor* by the Pauli repulsion ΔE_{Pauli}. Both are relatively small and unimportant. The electrostatic attraction is small because neither fragment has more than one valence electron causing little of the favorable overlap of one atom's charge distribution with the nuclei of the other atom. The Pauli repulsion is small because there is no contribution to this term from the two singly occupied valence AOs as they are occupied with electrons of opposite spin. Thus, the trend in the thermodynamic stability ΔE (or $\Delta H^{298} = -$BDE) of the H–M bond, *i.e.*, the weakening along Li, Na and K, can be related directly to covalent features in the bonding mechanism: the bond overlap between and mixing of the SOMOs that yield the electron-pair bond.

From K to Rb the trend is determined by a more involved and subtle interplay of factors, and we restrict ourselves to the main effect. The step from K to Rb involves the introduction of the first subvalence d shell, *i.e.*, 3d. This has relatively little effect on the spatial extent of the *n*s AO, which expands slightly. The bond overlap $\langle 1s \mid ns \rangle$ further decreases from K to Rb but more slightly so than before (from Na to K). Note, however, that the 1s + *n*s mixing in HRb remains substantial (see Fig. 2). In the end, the effect of the slight reduction in bond overlap is delicately overruled by that of the increase in stabilization of the electron stemming from the metal *n*s AO as the orbital energy $\varepsilon(ns)$ rises from −2.7 (K) to −2.5 eV (Rb): the orbital interaction ΔE_{oi} becomes somewhat more stabilizing (Table 4 and Fig. 3). The presence of the 10 electrons in the subvalence 3d shell has a slightly more pronounced effect on the

Pauli repulsion: going from K to Rb it becomes 2 kcal mol^{-1} more repulsive. This is the reason why overall the H–M bond strength continues to decrease.

The H–M bond is somewhat stronger than the C–M bond in methylalkali metal monomers.[9b] There are two important factors making the H–M bond stronger. One is the above-mentioned absence of either valence or core closed-shell AOs in hydrogen leading to an exceptionally small Pauli repulsion ΔE_{Pauli} with the alkali metal (which also has no valence closed-shell AOs!). Thus, for the H–M bond ΔE_{Pauli} is 3.2, 5.0, 5.6 and 7.7 kcal mol^{-1} along Li–Rb (see Table 4), whereas for the H_3C–M bond it amounts to 38.4, 27.8, 23.4 and 30.7 kcal mol^{-1} (see ref. 9*b*). In addition, the net C–M bond energy ΔE_{homo} contains a destabilizing contribution ΔE_{prep} of 7–10 kcal mol^{-1} associated with pyramidalizing the CH_3 group.[9b] Such a term does obviously not exist for the H–M bond for which the net bond energy ΔE_{homo} is equal to the interaction energy ΔE_{int} and very similar to the orbital interactions ΔE_{oi}.

It is also interesting to note that, in terms of orbital mixing, the H–M bond is more covalent than the C–M bond whereas based on group electronegativities of H and CH_3, one would expect the opposite.[9b] Thus, the electron-pair bonding MO of the H–M bond (*ca.* 63% hydrogen 1s + 26% metal *n*s) is less polarized toward the electronegative fragment than that of the C–M bond (*ca.* 70% methyl $2a_1$ + 25% metal *n*s) in spite of that fact that hydrogen (ε(1s) = −7.6 eV) is more electronegative than the methyl group ($\varepsilon(2a_1)$ = −6.5 eV for pyramidal CH_3) as indicated by the energies of the respective SOMOs. The exalted covalent character of the H–M is ascribed to the fact that the hydrogen 1s AO can build up a significantly larger overlap with the alkal imetal *n*s AO (0.51, 0.44, 0.37, 0.35 along Li–Rb, see Table 4) than the methyl $2a_1$ SOMO (0.31, 0.28, 0.21, 0.19 along Li–Rb, see ref. 9*b*), which directs only part of its amplitude toward the metal.

Finally, for an ionic bonding mechanism, one would expect a trend in orbital interactions that is opposite to that actually observed. If the H–M bond were predominantly ionic with marginal covalent contributions, the MO carrying the bonding electron pair would have only a slight contribution of the metal *n*s AO. In other words, this MO would resemble the hydride anion 1s AO rather than a bonding 1s + *n*s combination. Consequently, it would be hardly stabilized with respect to the hydrogen 1s atomic orbital. This ionic bonding mechanism is schematically shown in **8** ($\Delta\chi$ refers to the electronegativity difference defined in terms of the orbital-energy difference ε(1s) − ε(*n*s), see ref. 20):

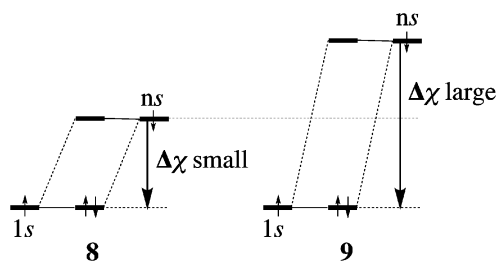

In this (fictitious) ionic picture, the electron simply drops from the metal *n*s AO into the hydrogen 1s AO giving rise to a stabilization that equals the orbital energy difference ε(1s) − ε(*n*s), indicated in **8** by a bold arrow. Thus, one would expect that the H–M orbital interaction ΔE_{oi} *increases* if the metal AO energy ε(*n*s) rises, that is, if the alkali metal becomes more electropositive, because, as shown in **9**, the electron originating from the metal would experience a larger stabilization energy ε(1s) − ε(n*s*). But, above, we have already seen that the opposite happens: the H–M orbital interaction ΔE_{oi} *decreases* (Table 4: ΔE_{oi} = −52.7, −40.4, −39.2 kcal mol^{-1}) as the metal becomes more electropositive (Fig. 3: ε(*n*s) = −3.3, −3.1, −2.7 along M = Li, Na and K, see also ref. 20).

In conclusion, the H–M bond has substantial covalent character (comparable to that of the C–M bond) stemming from bond overlap that determines the trend in bond strength as M descends the periodic table in Group 1. The fact that part of the stabilization stems from bond overlap is not in contradiction with this bond being highly polar.

Charge distribution

The metal atomic charge in HM first decreases from Li to Na and then increases again along Na, K and Rb according to both the VDD and Hirshfeld method (see Table 5). The VDD method, for example, yields values of +0.464, +0.458, +0.525 and +0.538 e along the series. This trend is similar to that for CH_3M molecules and, as explained in detail for the former,[9b] can be understood as resulting from the interplay of two effects. The first one is the increasing extent of charge separation that results when the hydrogen atom moves farther away from the metal atom as the latter increases along Li–Rb. Thus, the negative charge gained by the hydrogen atom due to the formation of the 1s + *n*s electron-pair bond penetrates less into the region of the metal atom and is increasingly associated with the former. Superimposed on this mechanism, which on its own would cause a steady increase of charge separation, there is a second effect, namely the loss (or strong reduction) of participation of the alkali metal np_σ AO if one goes from Li to Na. This counteracts the former mechanism because it increases the alkali metal atomic charge in HLi (and not in HNa) by enhancing the polarization of the electron-pair bonding MO toward the hydrogen atom. The trend in dipole moment μ increases systematically from 5.8 to 6.0 to 7.9 to 8.4 D along Li, Na, K and Rb in spite of the dip in the alkali metal atomic charge for sodium (Table 5). Thus, from Li to Na the trend in dipole moment is dominated by the increase in H–M bond length.

The above values indicate that the H–M bond is somewhat more polar than the C–M bond for which smaller metal atomic charges (VDD: +0.386, +0.351, +0.428 and +0.466 e) and dipole moments (5.6, 5.2, 6.9 and 7.7 D) have been computed.[9b] Note that this is so in spite of the fact that the electron-pair bonding combination of the H–M bond (*ca.* 63% hydrogen 1s + 26% metal *n*s) is less polarized toward the electronegative fragment than that of the C–M bond (*ca.* 70% methyl $2a_1$ + 25% metal *n*s). The origin of the somewhat higher atomic charges in HM is that the charge gained by the hydrogen 1s AO is not so much oriented toward the alkali metal atom as the charge gained by the methyl $2a_1$ orbital that penetrates more strongly across the bond midplane. Consequently, in the case of H–M a smaller fraction of the charge carried by the electron-pair bonding MO is associated with the alkali metal atom making the latter effectively more positive. This mechanism is illustrated by **10a** and **10b** (the dashed lines indicate the bond midplane).

Table 5 Metal atomic charge (in e) and dipole moment μ (in D) of alkali metal hydride monomers and tetramers[a]

	HLi	HNa	HK	HRb	$(HLi)_4$	$(HNa)_4$	$(HK)_4$	$(HRb)_4$
VDD	0.464	0.458	0.525	0.538	0.300	0.387	0.412	0.414
Hirshfeld	0.414	0.386	0.457	0.470	0.296	0.346	0.401	0.417
μ	5.805[b]	5.985[c]	7.949	8.426	0	0	0	0

[a] At BP86/TZ2P. [b] Exp: 5.882 ± 0.003 D, see ref. 7*e*. [c] Exp: 6.4 ± 0.7 D, see ref. 7*f*.

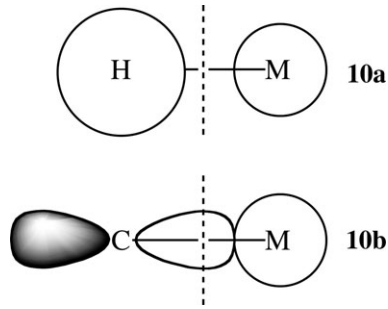

Heterolytic bond dissociation

So far, we have examined the extent of orbital mixing, its importance for trends in the bond strength and the polarity or charge separation in the H–M bond. Another criterion classifying the H–M bond as covalent is its intrinsic preference for dissociating homolytically and not heterolytically (*vide supra*). To enable a quantitative comparison with other bonds, we have computed the ratio of $\Delta E_{\text{hetero}}/\Delta E_{\text{homo}}$ as a measure for this preference using bond energy values from Table 2. The $\Delta E_{\text{hetero}}/\Delta E_{\text{homo}}$ ratios of HLi, HNa, HK and HRb are 2.9, 3.4, 3.1 and 3.0, respectively. These values are smaller than the $\Delta E_{\text{hetero}}/\Delta E_{\text{homo}}$ ratios of the corresponding C–M bonds of the methylalkali metal monomers (3.9, 5.0, 4.9 and 5.0) and that of the C–H bond in methane (3.8).[9b] Thus, according to this criterion, the H–M bond behaves somewhat less covalently than the C–M or C–H.

It is instructive to carry out an ionic analysis of the H–M bond, that is, a bond energy decomposition of the interaction between H^- and M^+ in HM (see Table 6) and to compare this with the analysis of the interaction between $H^\bullet$ and $M^\bullet$ in the same molecule (Table 4). In the ionic approach, the classical electrostatic attraction ΔV_{elstat} becomes the dominant bonding term with values that vary from −182.6 to −174.5 to −159.0 to −161.3 kcal mol^{-1} along Li–Rb (Table 6). On the other hand, the orbital interaction ΔE_{oi} becomes significantly smaller with values that vary from −20.3 to −15.4 to −12.3 to −13.2 kcal mol^{-1} along Li–Rb (Table 6). This has previously been interpreted as suggesting that, compared to the homolytic approach, the charge redistribution in the ionic analysis is smaller, that is, that the ionic fragments correspond more closely to the final charge distribution in the alkali metal molecule than the neutral methyl and alkali metal radical fragments.[17b] Another factor, not directly related to the extent of charge redistribution, that also contributes to the reduced ΔE_{oi} in the ionic analysis is the fact that we lose the stabilization associated with the electron dropping from the SOMO of the metal atom into the H–M bonding MO. The enormous increase in ΔV_{elstat} compared to the

Table 6 Analysis of the H–M bond between H^- and M^+ in alkali metal hydride monomers[a]

	H–Li	H–Na	H–K	H–Rb
ΔE_σ	−20.3	−15.4	−11.9	−12.6
ΔE_π	0.0	0.0	−0.4	−0.6
ΔE_{oi}	−20.3	−15.4	−12.3	−13.2
ΔE_{Pauli}	37.0	41.2	46.0	55.1
ΔV_{elstat}	−182.6	−174.5	−159.0	−161.3
$\Delta E_{\text{int}} = \Delta E_{\text{hetero}}$	−165.9	−148.7	−125.3	−119.4

[a] At BP86/TZ2P.

Table 7 Monomer–monomer bond energy (in kcal mol^{-1}) decomposition for alkali metal hydride tetramers[a]

	$(HLi)_4$	$(HNa)_4$	$(HK)_4$	$(HRb)_4$
ΔE_{oi}	−76.8	−71.4	−51.8	−49.5
ΔE_{Pauli}	152.5	133.2	134.6	164.3
ΔV_{elstat}	−225.0	−177.6	−195.7	−221.3
ΔE_{int}	−149.3	−115.8	−112.9	−106.5
ΔE_{prep}	12.8	18.8	11.6	9.2
ΔE_{tetra}	−136.5	−97.0	−101.3	−97.3

[a] At BP86/TZ2P.

homolytic approach (compare Tables 4 and 6) is of course due to the energetically unfavorable charge separation that we enforce by our choice to completely transfer one electron from one of the constituting fragments of HM to the other. It is perfectly valid to carry out such an analysis. One must be aware, however, that the results refer to the higher-energy process of heterolytic bond breaking and *not* to the energetically preferred homolytic bond dissociation.

3.4. Analysis of monomer–monomer interaction in HM tetramers

To understand the stability of the alkali metal hydride tetramers toward dissociation into the four monomers we have analyzed the interaction between these monomers in the tetramer. The decomposition of the tetramerization energy, shown in Table 7, reveals that the electrostatic attraction ΔV_{elstat} is the dominant bonding force. This term first decreases from −225.0 (HLi) to −177.6 (HNa) and increases thereafter to −195.7 (HK) and further to −221.3 kcal mol^{-1} (HRb). The sudden decrease of ΔV_{elstat} from the lithium hydride to the sodium hydride tetramer is caused by the combined effects of an increasing H–M distance (Table 1) and the decreasing atomic charge (Table 5) if one goes from Li to Na. This agrees with Rupp and Ahlrichs who attributed the decrease in tetramerization energy going from HLi to HNa to the increased interatomic distances in the latter.[8d] Along Na, K and Rb, the trend in ΔV_{elstat} parallels the trend of increasing charge separation as reflected by the atomic charges and the dipole moments collected in Table 7.

The orbital interactions ΔE_{oi} between the HM monomers, although much smaller than ΔV_{elstat}, are still important for the cohesion between the monomers, with values ranging from −76.8 kcal mol^{-1} for the lithium hydride tetramer to −49.5 kcal mol^{-1} for the rubidium hydride tetramer (Table 7). Note that these orbital interactions do not involve the formation of an electron-pair bond. They are provided by donor–acceptor interactions of the occupied σ_{H-M} orbitals (polarized toward H) with unoccupied σ^*_{H-M} orbitals (polarized toward M) of the monomers. Consequently, tetramerization reduces the charge separation because the donor–acceptor orbital interactions cause charge transfer from H to M. This is also confirmed by the VDD and Hirshfeld atomic charges, which are consistently smaller in $(HM)_4$ than in HM (see Table 5). The same phenomenon has also been observed for the corresponding methylalkali metal systems.[9b] The net interaction energy ΔE_{int} between HM monomers decreases along Li–Rb, steeply at first, from −149.3 (HLi) to −115.8 (NHa), and then more gradually to −112.9 (HK) and further to −106.5 kcal mol^{-1} (HRb). The main feature of this trend, that is, the steep decrease in monomer–monomer interaction from lithium hydride to the heavier alkali metal hydrides, is preserved in the overall tetramerization energies and enthalpies (see Tables 3 and 7). Tetramerization is somewhat more stabilizing for alkali metal hydrides HM (ΔH_{tetra} = −130.5 to −94.0 kcal mol^{-1}, along Li–Rb, Table 3) than for methylalkali metal molecules CH_3M (ΔH_{tetra} = −120.8 to −87.1 kcal mol^{-1}, see ref. 9*b*), amongst others because of less Pauli repulsion between the sterically less demanding HM monomers.

3.5. Covalency and ionicity: criteria and physical interpretation

In the above, we have discussed the nature of a series of H–M bonds, in particular the extent to which they behave "covalently" as opposed to "ionically". In the following, we elaborate more explicitly on these concepts as such. What is exactly meant with the "covalency" and "ionicity" of a bond? And to what extent can these properties be defined in a quantitative *and* physically meaningful manner? Let us begin by summarizing some of the quantities that we have analyzed above in order to examine the "covalency" (or "ionicity") of the H–M bonds: (i) the magnitude and *trend* in the orbital interaction ΔE_{oi}; (ii) the composition of the wavefunction (or the electron-pair bonding MO) in terms of H and M contributions; and (iii) the charge separation across the H–M bond. These are three, to some extent orthogonal aspects of the property of "covalency". They are determined by three main factors: (i) the bond overlap S_{bond} or, more precisely, the interaction matrix element F_{bond}, between the SOMOs of H and M; (ii) the electronegativity difference $\Delta\chi$ or, more precisely, the difference in SOMO energies of H and M; and (iii) the bond distance H–M.

One approach for classifying a bond as covalent or ionic is by determining which of the above factors dominates the energetics, that is, the magnitude of and, especially, the trend in H–M bond energies. Here, the bond overlap is the factor that can be associated with covalent character: if it dominates through the orbital interactions ΔE_{oi} the behavior, *e.g.*, trends in bond energies, the bond is considered covalent. On the other hand, the bond is conceived ionic if the electronegativity difference determines its behavior. It is clear that the electronegativity difference across all H–M bonds studied here is large and increases along Li–Rb. It is therefore not surprising that we and others find large positive charges on the metal atoms. In this study, we have also shown that these charges increase if the metal atom becomes more electropositive, as one might expect. Yet, the trend in H–M bond energies indicates genuine covalent character: it is determined by how the bond overlap changes along Li–Rb and not by the electronegativity difference (*vide supra*). This may come as a surprise, especially in light of most of the earlier literature, which on the basis of metal atomic charges would classify these bonds as predominantly, if not purely ionic. It may also seem somewhat contradictory. The point is that we are looking at two different properties, namely the mechanism through which the bond is stabilized and the extent of charge separation across this bond. They are both governed by one or more of the three factors mentioned above (*i.e.*, S_{bond}, $\Delta\chi$, distance H–M) but generally not in the same manner. The stabilization mechanism of the bond and the resulting charge separation are thus to some extent orthogonal. This means that one of them is not necessarily a hard indicator for the other one. Another consequence is that a high polarity or charge separation does not rule out that covalent factors such as the bond overlap dominate trends in H–M bond strengths.

Nevertheless, the polarity of chemical bonds is an important property and is often used as an alternative definition of "covalency" and "ionicity". One approach to quantify the polarity is computing the charge separation across the bond in terms of the charges of the atoms involved. The idea is that a completely covalent bond in a neutral molecule, say A–B, involves neutral atoms (or fragments) A and B whereas a completely ionic bond, in which one electron is completely transferred, is associated with atoms A^+ and B^- carrying opposite charges of $+1.0$ and -1.0 electrons, respectively. This can be carried out in a routine manner. Note, however, that atomic charges cannot be interpreted as absolute bond polarity indicators.[9b,17a] The problem originates from the fact that different atomic charge schemes have different scales, that is, the value of the computed charge of one particular atom in a molecule can vary significantly from one method to another. Atomic charges can still gain physical meaning but only in terms of trends, *i.e.*, by comparing relative magnitudes of atomic charges computed consistently with the same method. Only in this way, one can learn if a computed charge should be considered small, corresponding to an essentially covalent bond, or large, indicating increased ionic character. Thus, we can classify the H–Li bond as more polar (46% "ionic") than the H_3C–Li bond (39% "ionic") and less

polar than the H–Rb bond (54% "ionic") but it must be clear to which scale these numbers refer, in this example VDD (see Table 5 and ref. 9*b*). A similar picture emerges if we use, for example, the Hirshfeld scale, but with different absolute values.

We have recently proposed an alternative method[9b] of quantifying the bond polarity, which is based on the composition of the wavefunction in terms of H and M contributions. In particular, we look at the relative contribution x of the SOMO of one of the fragments, say the more electronegative one (here: the hydrogen atom), to the H–M electron-pair bonding MO. This approach is firmly rooted in MO theory and has the advantage over atomic charges that at least the range of values between the purely covalent and ionic situations is well defined.[22] Thus, the purely covalent situation occurs for $x = x_C = 0.5$: the radical electrons of both fragments pair-up in an electron-pair bonding combination of the overall molecule that has equal contributions from either fragment SOMO. The purely ionic situation occurs for $x = x_I = 1$: the unpaired electron of the metal atom is completely transferred to the methyl SOMO which transforms, without admixture of the metal AO, into a lone-pair-like MO in the overall molecule. The percentage covalency C and ionicity I is then defined as in eqn (6) and (7), respectively, with $I + C = 100\%$.

$$C = \frac{x_I - x}{x_I - x_C} \times 100\% \tag{6}$$

$$I = \frac{x - x_C}{x_I - x_C} \times 100\% \tag{7}$$

In Table 8, we have collected percentages of covalency C of the H–M bonds of our alkali metal hydride monomers based on eqn (6) using two ways of computing the fraction x. In the first one, x is the Gross Mulliken contribution of the hydrogen 1s SOMO to the electron-pair bonding combination in the overall molecule (see values in Fig. 2). The corresponding percentages for H_3C–M bonds are also listed in Table 8. Thus, we can classify the H–Li bond as more covalent (82% "covalent", 18% "ionic") than the H_3C–Li bond (60% "covalent", 40% "ionic") and of a similar polarity as the H–Rb bond (78% "covalent", 22% "ionic"). Note that the trend of increasing polarity along Li–Rb obtained on the basis of atomic charges essentially vanishes if we look at the composition of the electron-pair bonding MO. This difference is caused by the fact that the composition of the electron-pair bonding MO mainly depends on the electronegativity (or SOMO energy) difference whereas the actual charge separation is, in addition, strongly influenced by the H–M distance (the charge separation increases as the bond becomes longer).

There are still other ways of computing x, for example, on the basis of the Gross Mulliken population P (see values in Table 4) that the hydrogen 1s SOMO acquires in all occupied MOs of the overall molecule ($x = P/2$: see values in parentheses in Table 8), or on the basis of fragment MO *coefficients* (not shown in Table 8). Note

Table 8 Covalency C (in %) of H–M and C–M bonding in alkali metal hydride and methylalkali metal monomers[a]

M	H–M	C–M
Li	82 (82)	60 (60)
Na	72 (73)	58 (58)
K	66 (64)	54 (52)
Rb	78 (75)	58 (55)

[a] At BP86/TZ2P. C is computed with eqn (6) using for x the Gross Mulliken contribution of the hydrogen 1s or the methyl $2a_1$ SOMO to the electron-pair bonding combination (see values in Fig. 2 and ref. 9*b*). Value in parentheses: *idem*, using for x the Gross Mulliken Population P that the hydrogen 1s or the methyl $2a_1$ SOMO acquire in all occupied MOs of the overall molecule (see values in Table 4 and ref. 9*b*) divided by 2, *i.e.*, $x = P/2$.

that the particular values of C and I depend on how x is computed. One must be aware that this introduces again a certain arbitrariness making C and I semiquantitative rather than quantitative. Nevertheless, any choice for x produces the same trends in C and I, *i.e.*, a nearly constant extent of polarization of the H–M (or C–M) bond going from Li to the heavier alkali metals.

4. Conclusions

The H–M bond in alkali metal hydrides has substantial covalent character: it can well be viewed as an electron-pair bond between the singly occupied hydrogen and alkali metal valence-s AOs that gains substantial stabilization from the corresponding $\langle 1s \mid ns \rangle$ bond overlap. This is not in contradiction with this bond being highly polar as reflected by the dipole moment and atomic charges.

This follows from our BP86/TZ2P analyses of alkali metal hydride monomers HM and tetramers $(HM)_4$ with M = Li, Na, K and Rb. These analyses reveal significant orbital mixing in the H–M bond between the hydrogen 1s and alkali metal *n*s SOMOs (*ca.* 63% 1s + 26% *n*s) and the trend in bond strength is largely determined by the bond overlap $\langle 1s \mid ns \rangle$, which decreases along Li–Rb. Interestingly, the H–M electron-pair bonding MO is somewhat less polarized toward the electronegative fragment than that of the H_3C–M bond (*ca.* 70% $2a_1$ + 25% *n*s) although hydrogen is somewhat more electronegative than the methyl group. This is because of the larger bond overlap in HM. Our results also support the Valence-Bond analyses of Mo and Zhang who concluded that the Li–H bond is chiefly covalent.[5b]

A more general insight that evolves from our analyses is that bonding mechanism and polarity are two different, to some extent orthogonal qualities of a bond. While it is true that the polarity of a bond is the net result of the various features in the bonding mechanism, it is not true that this bonding mechanism and the relative importance of all its features (*e.g.*, electrostatic attraction, bond overlap, charge transfer) can be deduced from the bond polarity alone. Nevertheless, it is still common practice to use the terms "covalency" and "ionicity" for both aspects of a bond, its mechanism as well as its polarity, erroneously suggesting the equivalence of the latter. Therefore, we recommend to make explicit the precise definitions that one uses in the discussion of the "covalency" and "ionicity" of a bond.

Acknowledgements

We thank the following organizations for financial support: the HPC-Europa program of the European Union, the Deutsche Akademische Austauschdienst (DAAD), the Netherlands Organization for Scientific Research (NWO), the Ministerio de Educación y Ciencia (MEC), the Training and Mobility of Researchers (TMR) program of the European Union, the DURSI (Generalitat de Catalunya) and the National Research School Combination-Catalysis (NRSC-C). Excellent service by the Stichting Academisch Rekencentrum Amsterdam (SARA) and the Centre de Supercomputació de Catalunya (CESCA) is gratefully acknowledged. F. M. B. would like to thank Mr Willem-Jan van Zeist for presenting this paper in his name at the *Faraday Discussion* symposium held in Manchester, UK.

References

1 B. Ransil, *Rev. Mod. Phys.*, 1960, **32**, 239.
2 G. Rajagopal, R. N. Barnett and U. Landman, *Phys. Rev. Lett.*, 1991, **67**, 727.
3 B. K. Rao, S. N. Khanna and P. Jena, *Phys. Rev. B*, 1991, **43**, 1416.
4 H. Kato, I. Hirao, I. Nishida, K. Kimoto and K. Akagi, *J. Phys. Chem.*, 1981, **85**, 3391.
5 (*a*) M. Bertolus, V. Brenner and P. Millié, *J. Chem. Phys.*, 2001, **115**, 4070; (*b*) Y. Mo and Q. Zhang, *J. Phys. Chem.*, 1995, **99**, 8535.
6 (*a*) M. Hargittai, *Chem. Rev.*, 2000, **100**, 2233; (*b*) M. Hargittai and I. Hargittai, *The Molecular Geometries of Coordination Compounds in the Vapor Phase*, Elsevier, Amsterdam, 1997; (*c*) T. P. Martin, *Phys. Rep.*, 1983, **95**, 167.
7 (*a*) M. Dulick, K.-Q. Zhang, B. Guo and P. F. Bernath, *J. Mol. Spectrosc.*, 1998, **188**, 14; (*b*) J. F. Ogilvie, *J. Mol. Spectrosc.*, 1998, **180**, 193; (*c*) W. C. Stwalley, W. T. Zemke and

S. C. Yang, *J. Phys. Chem. Ref. Data*, 1991, **20**, 153; (*d*) W. C. Stwalley and W. T. Zemke, *J. Phys. Chem. Ref. Data*, 1993, **22**, 87; (*e*) L. Wharton, L. P. Gold and W. Klemperer, *J. Chem. Phys*., 1962, **37**, 2149; (*f*) P. J. Dagdigian, *J. Chem. Phys*., 1979, **71**, 2328; (*g*) M. Veith, P. König, A. Rammo and V. Huch, *Angew. Chem*., 2005, **117**, 6123; (*h*) M. Veith, P. König, A. Rammo and V. Huch, *Angew. Chem., Int. Ed*., 2005, **44**, 5968.

8 (*a*) J. Breidung and W. Thiel, *J. Mol. Struct*., 2001, **599**, 239; (*b*) V. Bonacic-Koutecky, J. Pittner and J. Koutecky, *Chem. Phys*., 1996, **210**, 313; (*c*) F. Moscardó, A. J. Pérez-Jiménez and A. Cjuno, *J. Comput. Chem*., 1998, **19**, 1899; (*d*) M. Rupp and R. Ahlrichs, *Theor. Chim. Acta*, 1977, **46**, 117; (*e*) M. Dolg, *Theor. Chim. Acta*, 1996, **93**, 141; (*f*) T. Kremer, S. Harder, M. Junge and P. v. R. Schleyer, *Organometallics*, 1996, **15**, 585; (*g*) P. Fuentealba and A. Savin, *J. Phys. Chem. A*, 2001, **105**, 11531; (*h*) P. Fuentealba and O. Reyes, *J. Phys. Chem. A*, 1999, **103**, 1376; (*i*) H. Kato, K. Hirao and K. Akagi, *Chem. Phys. Lett*., 1981, **77**, 580; (*j*) H. Kato, K. Hirao and K. Akagi, *Inorg. Chem*., 1981, **20**, 3659; (*k*) E. S. Sachs, J. Hinze and N. H. Sabelli, *J. Chem. Phys*., 1975, **62**, 3367; (*l*) J. W. Ochterski, G. A. Petersson and K. B. Wiberg, *J. Am. Chem. Soc*., 1995, **117**, 11299; (*m*) B. H. Cardelino, W. H. Eberhardt and R. F. Borkman, *J. Chem. Phys*., 1986, **84**, 3230; (*n*) F. Weigend and M. Häser, *Theor. Chem. Acc*., 1997, **97**, 331.

9 (*a*) F. M. Bickelhaupt, M. Solà and C. Fonseca Guerra, *J. Mol. Model*., 2006, **11**, 563; (*b*) F. M. Bickelhaupt, M. Solà and C. Fonseca Guerra, *J. Chem. Theor. Comput*., 2006, **2**, 965.

10 F. M. Bickelhaupt and E. J. Baerends, in *Rev. Comput. Chem*., ed. K. B. Lipkowitz and D. B. Boyd, Wiley-VCH, New York, 2000, vol. 15, pp. 1–86.

11 (*a*) G. te Velde, F. M. Bickelhaupt, E. J. Baerends, S. J. A. van Gisbergen, C. Fonseca Guerra, J. G. Snijders and T. Ziegler, *J. Comput. Chem*., 2001, **22**, 931; (*b*) C. Fonseca Guerra, J. G. Snijders, G. te Velde and E. J. Baerends, *Theor. Chem. Acc*., 1998, **99**, 391; (*c*) C. Fonseca Guerra, O. Visser, J. G. Snijders, G. te Velde and E. J. Baerends, in *Methods and Techniques for Computational Chemistry*, ed. E. Clementi and G. Corongiu, STEF, Cagliari, 1995, pp. 305–395; (*d*) E. J. Baerends, D. E. Ellis and P. Ros, *Chem. Phys*., 1973, **2**, 41; (*e*) P. M. Boerrigter, G. te Velde and E. J. Baerends, *Int. J. Quantum Chem*., 1988, **33**, 87; (*f*) G. te Velde and E. J. Baerends, *J. Comput. Phys*., 1992, **99**, 84; (*g*) J. G. Snijders, E. J. Baerends and P. Vernooijs, *At. Nucl. Data Tables*, 1982, **26**, 483; (*h*) J. Krijn and E. J. Baerends, *Fit Functions in the HFS Method Internal Report (in Dutch)*, Vrije Universiteit, Amsterdam, 1984.

12 (*a*) L. Versluis and T. Ziegler, *J. Chem. Phys*., 1988, **88**, 322; (*b*) L. Fan and T. Ziegler, *J. Chem. Phys*., 1991, **95**, 7401; (*c*) G. Schreckenbach, J. Li and T. Ziegler, *Int. J. Quantum Chem*., 1995, **56**, 477.

13 L. Fan, L. Versluis, T. Ziegler, E. J. Baerends and W. Ravenek, *Int. J. Quantum Chem. Symp*., 1988, **22**, 173.

14 (*a*) A. D. Becke, *J. Chem. Phys*., 1986, **84**, 4524; (*b*) A. Becke, *Phys. Rev. A*, 1988, **38**, 3098; (*c*) J. P. Perdew, *Phys. Rev. B*, 1986, **33**, 8822; (*d*) J. P. Perdew, *Phys. Rev. B*, 1986, **34**, 7406; (*e*) L. Fan and T. Ziegler, *J. Chem. Phys*., 1991, **94**, 6057.

15 P. W. Atkins, *Physical Chemistry*, Oxford University Press, Oxford, 1982.

16 (*a*) K. J. Morokuma, *Chem. Phys*., 1971, **55**, 1236; (*b*) K. Kitaura and K. Morokuma, *Int. J. Quantum Chem*., 1976, **10**, 325; (*c*) F. M. Bickelhaupt, N. M. M. Nibbering, E. M. van Wezenbeek and E. J. Baerends, *J. Phys. Chem*., 1992, **96**, 4864; (*d*) T. Ziegler and A. Rauk, *Inorg. Chem*., 1979, **18**, 1558; (*e*) T. Ziegler and A. Rauk, *Theor. Chim. Acta*, 1977, **46**, 1.

17 (*a*) C. Fonseca Guerra, J. W. Handgraaf, E. J. Baerends and F. M. Bickelhaupt, *J. Comput. Chem*., 2004, **25**, 189; (*b*) F. M. Bickelhaupt, N. J. R. van Eikema Hommes, C. Fonseca Guerra and E. J. Baerends, *Organometallics*, 1996, **15**, 2923.

18 See also: (*a*) C. Fonseca Guerra, F. M. Bickelhaupt, J. G. Snijders and E. Baerends, *Chem.–Eur. J*., 1999, **5**, 3581; (*b*) C. Fonseca Guerra and F. M. Bickelhaupt, *J. Chem. Phys*., 2003, **119**, 4262. Voronoi cells are equivalent to Wigner–Seitz cells in crystals; for the latter, see; (*c*) C. Kittel, *Introduction to Solid State Physics*, Wiley, New York, 1986.

19 F. L. Hirshfeld, *Theor. Chim. Acta*, 1977, **44**, 129.

20 J. B. Mann, T. L. Meek and L. C. Allen, *J. Am. Chem. Soc*., 2000, **122**, 2780.

21 The description of the MO in terms of fragment MO *coefficients* instead of Gross Mulliken contributions yields the same picture but it has the disadvantage of not being normalized, that is, the figures do not add up to 1 (or to 100%).

22 T. A. Albright, J. K. Burdett and M. Whangbo, *Orbital Interactions in Chemistry*, Wiley, New York, 1985.

23 The H–M bond distance also increases along Li–Rb because of the increasing number of metal core shells that enter into Pauli repulsion with closed shells on the methyl fragment. For a discussion on how the interplay of bonding and repulsive orbital interactions determines bond lengths, see for example: F. M. Bickelhaupt, R. L. DeKock and E. J. Baerends, *J. Am. Chem. Soc*., 2002, **124**, 1500.

